Cement and Concrete Composites 124 (2021) 104260

Contents lists available at ScienceDirect

Cement and Concrete Composites

journal homepage: www.elsevier.com/locate/cemconcomp

Use of scratch tracking method to study the dissolution of alpine aggregates subject to alkali silica reaction

Mahsa Bagheri [a,*], Barbara Lothenbach [b], Mahdieh Shakoorioskooie [b,c,d], Andreas Leemann [b], Karen Scrivener [a]

[a] Laboratory of Construction Materials, EPFL, 1015, Lausanne, Switzerland
[b] Concrete and Asphalt Laboratory, Empa, Swiss Federal Laboratories for Materials Science and Technology, CH-8600, Dübendorf, Switzerland
[c] Institute for Building Materials (IfB), ETH Zürich, CH-8093, Zürich, Switzerland
[d] Center for X-ray Analytics, Empa, Swiss Federal Laboratories for Materials Science and Technology, CH-8600, Dübendorf, Switzerland

ARTICLE INFO

Keywords:
Aggregate dissolution
The scratch-tracking method
ASR expansion
Alkali effect

ABSTRACT

Alkali silica reaction (ASR) can significantly affect the service life of concrete. The dissolution of aggregates has a direct impact on gel formation and thus on the macroscopic expansion. The conventional expansion tests and other investigations confirmed ASR reactivity of three aggregates from different locations in Switzerland. The reactive minerals within alpine and composite aggregates were identified using an innovative scratch-tracking method. This method helps to study aggregate dissolution if measuring the amount of released Si is not enough, because: several minerals release Si or Al and/or new phases are probable to form during dissolution experiment. The scratch-tracking method on theses alpine aggregates showed faster dissolution of feldspars and quartz while muscovite was hardly affected. The dissolution of the aggregates in solution confirmed these differences between minerals.

1. Introduction

Alkali-silica reaction (ASR) can cause serious problems for the durability of concrete. ASR is a chemical reaction between SiO_2-containing minerals within aggregates and the alkaline pore solution of concrete. The formation of reaction products leads to cracking of the aggregates; the cracking usually starts inside the aggregates and then propagates into the cement paste [1–5]. The most widely accepted way to assess the alkali silica reaction is through its impact on expansion in mortar bars or concrete prisms [6]. ASR starts with aggregate dissolution, and this is an important parameter affecting expansion. Aggregate dissolution in concrete occurs mainly at the grain boundaries, where amorphous or poorly crystalline materials is found [1].

Slowing down of aggregate dissolution causes the formation of less ASR products, lowering the risk of damage due to ASR. To better understanding aggregate dissolution, particularly in complex aggregate containing many minerals, it is necessary to clearly identify which minerals are most reactive and how their reactivity is influenced by pH values and the presence of other ions.

Typical alpine aggregates contain different minerals such as quartz, feldspar, mica, chlorite, dolomite, and calcite. These minerals have very different dissolution rates in alkaline solution [7]. Usually only reactive silicates such as amorphous SiO_2 and poorly crystalline forms of quartz are considered to be susceptible to ASR [8]. However feldspar has a similar dissolution rate to quartz at high pH [7]. If feldspar dissolves, the release of alkali may speed up dissolution and/or the release of Al may slow it down [9].

If aggregate dissolution is studied in alkaline solution by measuring the amount of released ions, the parallel dissolution of other minerals (such as calcite [10]) may lead to the formation of new solids. For example, calcium silicate hydrates can precipitate with dissolved Si from silica-containing minerals, so following the amount of released Si is meaningless. Additionally, it is impossible to determine the source of the measured Si (or other components), if a composite aggregate contains different minerals with the common components. For instance if quartz and feldspars dissolve, both will released Si into the solution. These issues clarify that a new method is needed to study aggregate dissolution at high pH.

* Corresponding author.
E-mail addresses: mahsa.bagheri@epfl.ch, mahsa.bagheri@epfl.ch (M. Bagheri), barbara.lothenbach@empa.ch (B. Lothenbach), mahdieh.shakoorioskooie@empa.ch (M. Shakoorioskooie), andreas.leemann@empa.ch (A. Leemann), karen.scrivener@epfl.ch (K. Scrivener).

https://doi.org/10.1016/j.cemconcomp.2021.104260
Received 29 March 2021; Received in revised form 25 July 2021; Accepted 12 September 2021
Available online 20 September 2021

In the present study, three aggregates from different locations in Switzerland, Uri, Brienz and Praz (U, B and P), were assessed by expansion tests of concrete samples at 38 °C. These Swiss aggregates are known as ASR-reactive aggregates (Fig. A1) based on the concrete prism test (CPT) [11–13].

The major innovation of this paper is the use of a scratch-tracking method to identify the reactive minerals in the different aggregates. The results from this new method are critically compared to the more conventional method of studying the overall dissolution of the aggregates.

2. Materials and methods

2.1. Aggregate characterization

0.5 kg of each aggregate was taken from a well–mixed batch (size fraction of 0–4 mm), and was ground for X–ray fluorescence (XRF) analysis, using fused beads method according to EN 196–2. Total carbon content was determined by combustion analysis according to ISO 10694 and used to calculate the CO_2 content. For X-ray Powder Diffraction (XRD), a representative portion of each aggregate, from a well–mixed batch, was crushed and sieved between 0.315 and 0.630 mm, washed with water to remove any fine particles, and dried at 100 °C for 1 day. Samples of 20 g were taken randomly and ground to obtain fine powder (particle size distribution between 15 and 20 μm) for XRD analysis. A PANalytical X'Pert Pro MPD diffractometer with CuK$\alpha_{1,2}$ radiation was used to record the patterns. All the diffractograms were recorded between 5° and 70° 2Θ over 30 min with a step size of 0.017°, diverge slit 1/2°, mask 15 mm and soller slit 0.04 rad. After recording the patterns, Rietveld analyses were done to quantify the crystalline composition of the samples.

Thin–section petrographical investigations were made on all the aggregates using optical microscopy with crossed polarizers and inserted gypsum plate (CP–OM) to study texture and mineralogy of the aggregates. The CP-OM images of the thin cross-sections of concrete samples (with U, B and P aggregates) were recorded from the most representative microstructure (observed in more than 80% of the pieces).

2.2. Methods

2.2.1. Expansion test

Concrete prisms with standard size of 40 × 40 × 160 mm^3 were produced with U, B and P aggregates. An aggregate mass of 1790 kg/m^3 was used in the mix, with the following grain size distribution: 0–4 mm (40 wt %), 4–8 mm (25 wt %) and 8–11 mm (35 wt %). All specimens were cast using 440 kg/m^3 of Portland cement (CEM I/42.5 N) and with water to cement mass ratio of 0.5. The specimens were kept at 100% relative humidity for 24 h before unmolding. The expansion tests were done as described in detail in Ref. [14], which included immersion of the concrete prisms in an alkaline solution (a mix of 0.3 M KOH and 0.1 M NaOH to simulate the alkalinity of the pore solution within concrete, which is very close the composition of the extracted pore solution from concrete samples after 28 days) to prevent alkali leaching. The specimens were stored at 38 °C and the length changes of at least 10 specimens for each type of aggregate were regularly measured up to 250 days (9 months). A slice of each specimen with thickness of around 1 cm was cut at desired time and dried at 50 °C overnight. The sample was impregnated under vacuum in epoxy resin and left at room temperature to be harden for 1 day. The samples were polished up to 1 μm using diamond spray and polishing disc and coated with carbon for SEM analysis. Scanning electron microscopy (SEM) imaging (Thermo Scientific™ Quanta™ 650, pressure between 3.0 and 5.0 × 10^{-6} Torr) and energy dispersive X–ray (EDX) point analysis (Thermo Noran Ultra Dry 60 mm^2 detector and Pathfinder X-Ray Microanalysis Software) were used to track formation of the ASR products and study their chemical composition for all aggregate types at 56 and 250 days.

2.2.2. Identification and dissolution rate of reactive minerals

In order to identify which minerals dissolve in the aggregates, all three aggregates (U, B and P) were studied in two series of experiments a) the scratch-tracking method and b) dissolution in solution.

2.2.2.1. The scratch-tracking method

It is possible to directly observe dissolution of polished surfaces by SEM and EDX (to identify the chemical composition of the dissolved minerals). Randomly selected pieces of aggregates were impregnated in epoxy and after hardening; these were polished down to ¼ μm (with diamond sprays). The polished samples were cleaned several times by isopropanol and then deionized (DI)-water ultrasonically to remove any fine particles and impurities (Fig. A2). Then the samples were coated with carbon. The silica-containing areas (such as quartz, Na–feldspar, K–feldspar and muscovite) and calcite areas were found by EDX analysis. SEM secondary electron images from these areas of interest (at least five areas for each mineral) were recorded as reference images before doing dissolution experiments. After collecting the reference images, the carbon coating was removed by gently polishing for 2–3 min with a soft polishing cloth (OP-Nap, Struers) and petroleum lubricant. The samples were cleaned ultrasonically with DI-water and isopropanol three times each, and dried in the oven at 50 °C for 1 day. The samples were recoated and observed in the SEM to check whether the carbon-removing procedure produced any visible changes. The coating was then removed again and the samples were immersed in 0.4 M KOH solution at 38 °C for 21 and 60 days. After each period of dissolution, the samples were washed gently with isopropanol, dried, coated with carbon and re–examined in the SEM. After each SEM and EDX investigations, the carbon coating was removed as explained previously and was put back in the fresh 0.4 M KOH solution. Ultra-pure water was used for the preparations of all solution. The SEM images from the surface of the specimens after 21 and 60 days were aligned with respect to the first image of the same region using a rigid body registration (alignment) algorithm. Registration was conducted using a Python interface of SimpleElastix image registration library provided by Insight Segmentation and Registration Toolkit (ITK), based on a mutual information similarity metric [15]. To quantitatively compare the dissolution degree at different times (21 and 60 days), a threshold was applied to the aligned grey level SEM images to segment the scratches. The changes in the width size distribution (nm) and area fraction (%) were computed for segmented scratches.

2.2.2.2. Dissolution in solution

The homogeneity of the five subsamples of P aggregate (fine powder, obtained by grinding of 20 g of crushed aggregate with size fraction 0.315–0.630 mm) was checked by XRF and XRD analyses. The 5 subsamples showed very low deviation, confirming the homogeneity for dissolution experiments (Table A2). To study the type and amount of the dissolved ions from each aggregate at high pH, 20 g was put in either 120 ml of 0.4 M KOH or 0.4 M NaOH solution (to be able to measure both released Na and K) and stored at 38 °C. After different reaction times, an aliquot of the solution (5 ml) was sampled, and filtered with 0.2 μm nylon micro filter. 1 ml of the solution was diluted by a factor of 10 using ultra–pure water to avoid any precipitation (without acidification), and measured by Inductively Coupled Plasma Optical Emission Spectrometry (ICP–OES (Shimadzu ICPE–9000)) and Ion Chromatography (IC (Thermo Scientific Intergrion HPIC)). The amount of released component (wt. %) from each aggregate in 0.4 M KOH and 0.4 M NaOH was calculated by Eq. (1):

$$\text{Released component (wt. \%)} = \left(\frac{C_t \times V_{sol}}{W}\right) \times 100 \quad (1)$$

where C_t is the concentration of released component (g/l) from U, B and P aggregates at any time, V_{sol} is the solution volume (l) and W is the mass of available crystalline amount of the component (g) existing in 20 g of each aggregate before dissolution (calculated based on XRD Rietveld results). As dissolvable SiO_2 was provided from both quartz and feldspars, the total initial SiO_2 before dissolution was calculated considering both, based on the amount determined by XRD/Rietveld analysis and taking into account the fraction of SiO_2 in quartz and feldspars.

A pH meter (Lab 850) (with electrode BlueLine 14 pH (SI Analytics)), calibrated against standard solutions, was used to record pH values at ambient temperature. At the end of the dissolution experiments, the solids were collected by filtration, washed with ultra–pure water and isopropanol to remove the remaining KOH or NaOH solution and dried at 38 °C, and were analysed by XRD and thermogravimetric analysis (TGA) to check for any precipitation during the dissolution experiments (for example Fig. A5).

3. Results

3.1. Aggregate characterization

The XRD and XRF results of U, B and P aggregates are summarised in Table 1. The XRF analysis indicates that silica is the dominant oxide in all studied aggregates; the B aggregate contains more aluminium than U and P aggregates. Based on the Rietveld analysis, U and P aggregates contain around 50 wt % of quartz (SiO_2) and 26 wt % and 16 wt % of potassium and sodium feldspars ($KAlSi_3O_8$ or $NaAlSi_3O_8$), while B aggregates consist of about 25 wt % quartz and 50 wt % of feldspars.

Fig. 1 shows illustrative CP–OM images of the thin cross-sections of the concretes produced out of U, B and P aggregates at 14 days. The uniformly dark blue areas are the paste areas. Microstructures of P (Fig. 1 (a and d)) and B aggregates (Fig. 1 (b and e)) are quite similar and both of them are granitic. A bimodal grain size distribution of coarse quartz grains with highly undulose extinction can be observed in both P and B aggregates. However, the quartz grains are more elongated in P aggregate and more isometric in B aggregate. The matrix between the quartz grains consists of a mixture of muscovite and microcrystalline quartz. The U aggregate is a sedimentary rock and shows a significantly different texture. Coarse and microcrystalline quartz grains both with little undulose extinction and isometric form are present. Mica flakes are uniformly distributed in the interstitial regions between quartz grain boundaries. Amorphous silica exists at the quartz grain boundaries (Fig. 1 (c)), as reported in Ref. [16]. Calcite is detected by XRD and was also identified in the CP–OM images of all aggregates (Fig. 1 (d, e and f)). For P and B aggregates (Fig. 1 (d) and (e)), it was observed mainly as individual particles containing a mixture of quartz and calcite. However, in the case of U, calcite occurs mainly as detrital component in a size similar to the coarse quartz. Rarely, it is present as sparitic veins (Fig. 1 (f)).

Table 1
Chemical and mineralogical composition of the U, B and P aggregates.

Technique	Component	U	B	P
XRF (wt. %)	SiO_2	64.3	69.1	68.0
	Al_2O_3	8.8	14.3	7.2
	CaO	8.7	2.9	8.9
	K_2O	2.1	3.4	2.2
	MgO	2.1	1	1.9
	Fe_2O_3	2.0	2.3	1.4
	Na_2O	1.7	3.7	1.4
	SO_3	0.4	0.1	0.1
	LOI	9.5	2.6	8.7
XRD (wt. %)	**Quartz**: SiO_2 [ICSD 174]	49.7	24.9	55.5
	Feldspar: Albite: $NaAlSi_3O_8$ [ICSD 87657]	17.7	33.3	8.2
	Feldspar: Microcline: $KAlSi_3O_8$ [ICSD 83531]	7	11.7	7.9
	Feldspar: Orthoclase: $KAlSi_3O_8$ [ICSD 9543]	–	5.9	–
	Mica: Muscovite$KAl_2(AlSi_3O_{10})(OH)_2$ [ICSD 75952]	8.5	10.7	7.4
	Calcite: $CaCO_3$ [ICSD 73446]	6.8	10.4	15.2
	Dolomite: $CaMg(CO_3)_2$ [ICSD 66333]	6.5	0.3	4.5
	Chlorite: Clinochlore $Mg_5Al(AlSi_3O_{10})(OH)_8$ [ICSD 66258]	0.8	2.4	–
	Amorphous/non-crystalline	3	0.4	1.3

3.2. Concrete expansion

The relative length (Fig. 2) and mass (Fig. A3) changes of concrete prisms produced with three types of aggregates were measured as a function of time. The concrete sample with U aggregate showed the highest increase in length and mass. Since the samples were submerged in an alkaline solution (0.3 M KOH and 0.1 M NaOH), the expansion continuously increased over the course of 250 days. This behavior is in contrast with the conventional concrete performance laboratory–based tests [17,18] where reactions slow down after a certain time due to leaching of alkalis. In the case of concrete produced from U aggregates, the rate of expansion slowed down after 112 days. This is probably due to the extent of damage and crack filling, which is not investigated further here. SEM and EDX examinations of the cross-section of concrete samples after 250 days confirmed the formation of ASR products. The ASR-product compositions in all samples (Fig. A4) were similar to field and laboratory values, which were previously reported [19].

SEM images of the concretes were examined at 56 days and 250 days (Fig. 3). At 56 days the ASR products have formed at the grain boundaries of the different minerals (Fig. 3 (a, b and c)). This causes opening of cracks between the grains. After 250 days several larger cracks opened in the aggregates, Fig. 3 (d, e and f). The ASR gel exudes into the cement paste, where it takes up calcium [20].

3.3. Identification and dissolution rate of reactive minerals

3.3.1. The scratch-tracking method

Fig. 4 shows SEM secondary electron images of quartz, muscovite, K-feldspar and Na-feldspar areas of the P aggregate (a, d and g) before dissolution, (b, e and h) after 21 days and (c, f and i) after 60 days of immersion in 0.4 M KOH at 38 °C.

In the SEM images before immersion, it is just possible to see some weak scratches from the polishing process (Fig. 4 (a, d and g)). During immersion in the alkaline solution, the scratches in quartz, K–feldspar and Na–feldspar areas deepened and widened, and in addition, obvious dissolution occurred at the grain boundaries, while muscovite showed negligible changes after immersion in the alkali solution for 21 and 60 days (Fig. 4 (b and c), 4 (e and f) and 4 (h and i)). Additionally, there was severe dissolution of some calcite grains at the high pH as shown in Fig. 5. The calcite dissolution may be attributed to the absence of Ca in the solution. In concrete, where calcium is present from portlandite, very little dissolution of calcite is expected.

Fig. 4 (c, f and i) shows some precipitation on the sample surface after 60 days of immersion, which can be either ASR products or C–S–H (due to reaction of released Si from quartz and feldspars dissolution and released Ca from calcite dissolution). It was not possible to determine the chemical composition by EDX analysis because of the small amounts.

Fig. 4 (j) shows an example of alignment of SEM images (Fig. 4 (g) to 4 (i)) to quantify the dissolution extent based on the changes in the scratch width for quartz and K–feldspar areas of P aggregate. Fig. 6 shows (a) scratch width size distribution (nm) for quartz areas and (b) scratch area fraction (%) for quartz, K–feldspar, Na–feldspar and muscovite areas before dissolution of P aggregate and after 21 and 60 days of immersion. In the width distribution histograms for the quartz areas (Fig. 6 (a)), the peak of the fitted Gaussian distribution plot shifts to higher after 21 and 60 days. Before immersion, the average scratch width was around 50 nm, after dissolution for 21 days and 60 days this increased to approximately 85 nm and 135 nm respectively. Fig. 6 (b)

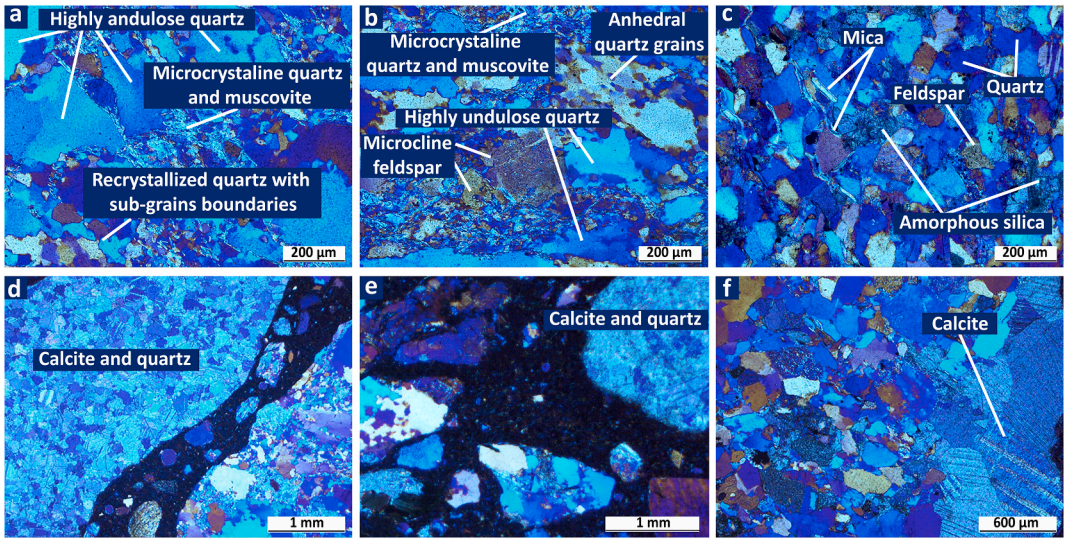

Fig. 1. CP–OM images of P (a and d), B (b and e) and U (c and f) aggregates.

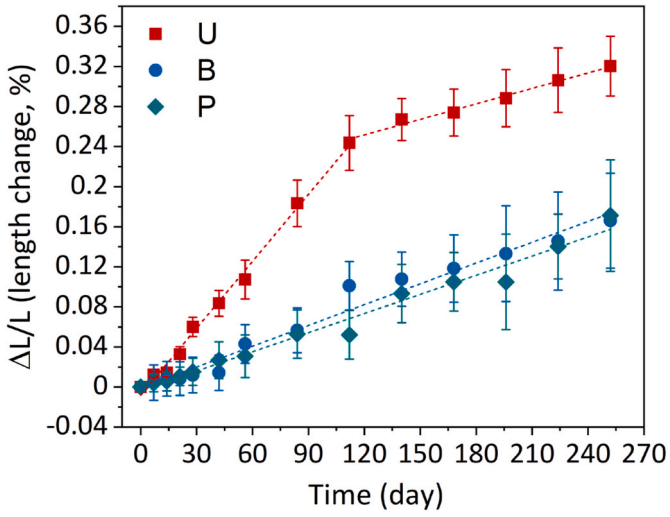

Fig. 2. Relative length change (%) of different concrete samples produced with U, B and P aggregates as a function of time.

indicates similar dissolution rates in quartz, K–feldspar and Na–feldspar areas, while a very slow dissolution of muscovite is observed. The reactivity of muscovite agrees with that reported by Leemann and Holzer [8]. However, they observed a higher reactivity of quartz compared to K–feldspar, this may be related to different feldspar polymorphs being present in the samples of this study.

Dissolution data for minerals at high pH values are scarce. Fig. 7 shows dissolution rates of quartz, Na–feldspar (albite) and K–feldspar as a function of pH ($9 < pH < 13$) at 25 °C from previous studies. At pH 12.3 and 25 °C, comparable dissolution kinetics for quartz ($5.4\ 10^{-11}$ mol/(m^2.s)) as for Na-feldspar (albite, $4.2\ 10^{-11}$ mol/(m^2.s)) were reported, while the one for K-feldspar at pH 12.7 and 25 °C ($0.5\ 10^{-11}$ mol/(m^2.s)) was somewhat slower (Fig. 7) [7,21–26]. Reported dissolution rates of muscovite at high pH are much lower ($\approx 10^{-12}$ mol/(m^2.s)) [27,28], in agreement with the observations made in this study. In this topography study using the scratch-tracking method, the scratches from polishing process were preferential areas for mineral dissolution, but comparative results are in good agreement with previous studies.

3.3.2. *Dissolution kinetics of aggregates*

The ICP-OES results showed linear increases of Si concentrations with time for all aggregates immersed in 0.4 M KOH and 0.4 M NaOH

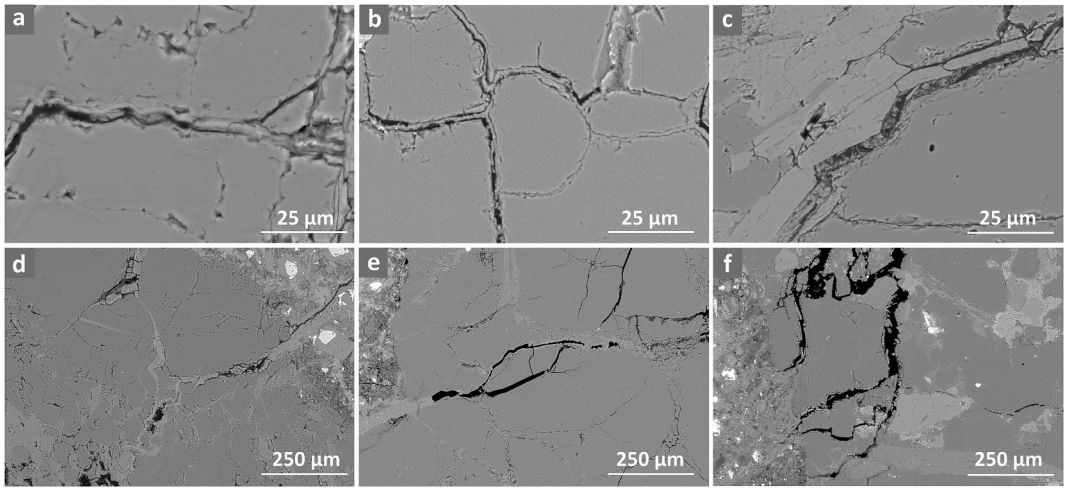

Fig. 3. SEM backscattered images of the cross-section of concrete samples with (a) P (b) B (c) U aggregates after 56 days, and (d) P (e) B (f) U aggregates after 250 days.

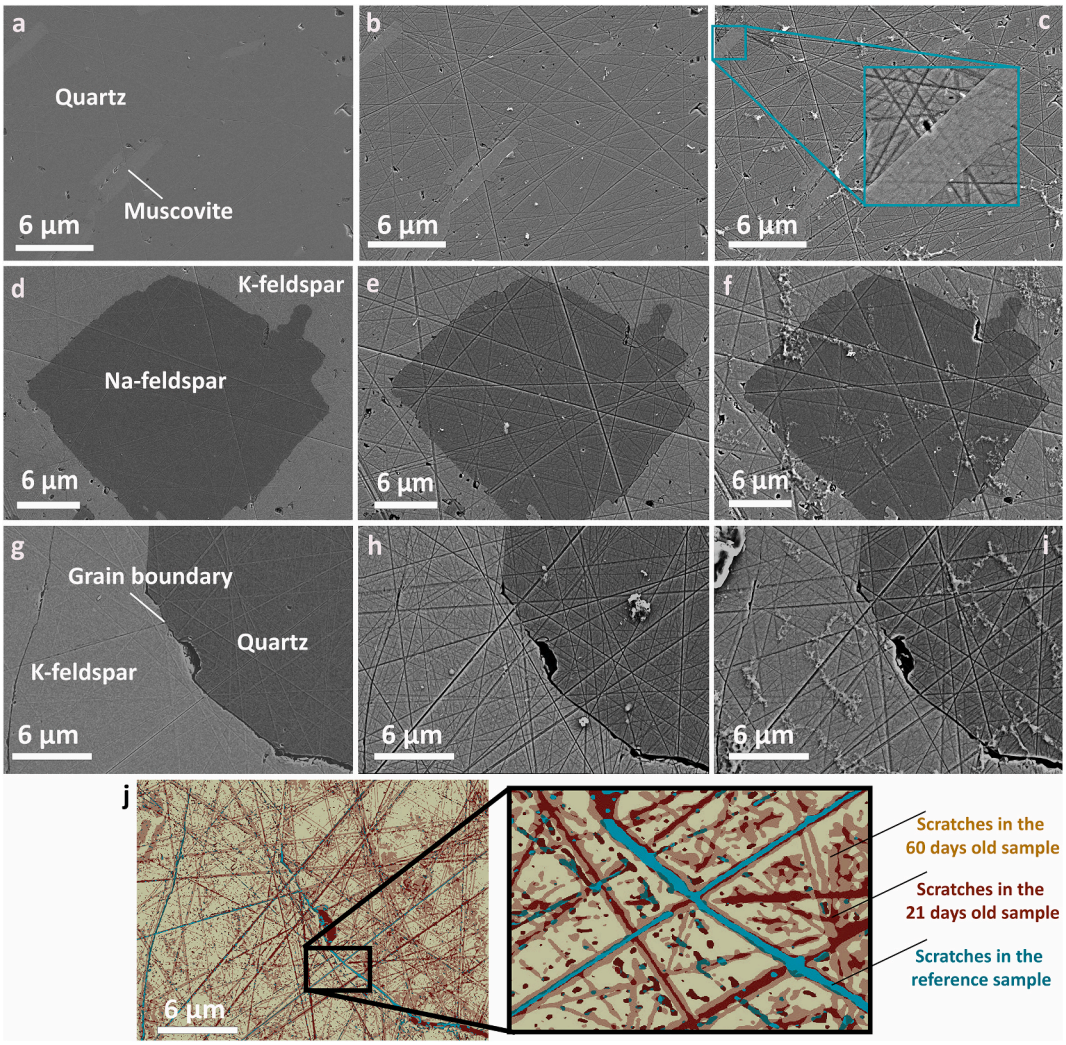

Fig. 4. Aligned SEM secondary electron images of (a, b and c) quartz and muscovite, (d, e and f) K–feldspar and Na–feldspar and (g, h and i) quartz and K–feldspar areas of P aggregate (a, d and g) before dissolution, (b, e and h) after 21 days and (c, f and i) 60 days of dissolution in 0.4 M KOH solution at 38 °C and j) overlapped image of segmented scratches in all the three SEM images (g–i) to quantify the width changes over time by dissolution increment.

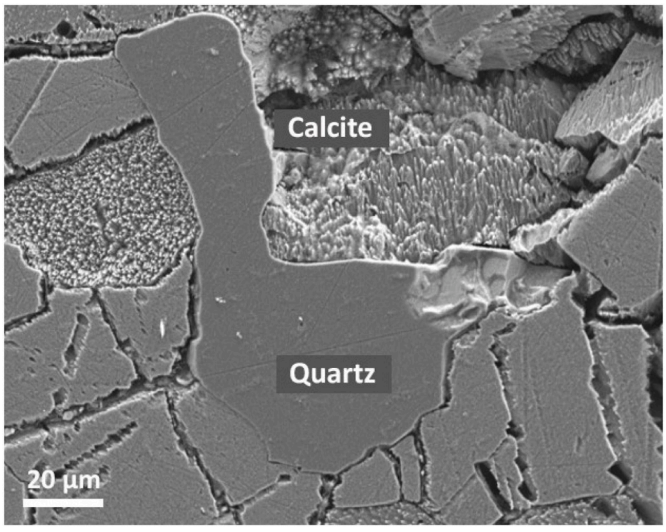

Fig. 5. SEM secondary electron images of quartz (darker grey area) and calcite (lighter grey area) areas of P aggregate after 60 days immersion in 0.4 M KOH solution at 38 °C.

(Table A3). The amount of SiO_2 dissolved for each measurement was calculated per g/l by Eq. (1). Since the topography study using the scratch-tracking method indicated the preferential dissolution of quartz and feldspars (in section 3.3.1), *W* in Eq. (1) was considered as the total mass of SiO_2 from quartz and feldspars before dissolution of the 20 g sample, based on the XRD Rietveld analysis (Table 1). All three aggregates have approximately similar content of silica based on the XRF analysis and total amount of quartz and feldspars from XRD (Table 1).

Fig. 8 indicates a linear increase of released SiO_2 (wt. %) for U, B and P aggregates. The U aggregate released the most silicon in both solution with more in 0.4 M KOH (0.48% after 63 days) than in 0.4 M NaOH (0.34% after 63 days) (Fig. 8 and Table A3), in agreement with the observations on quartz and silica [29,30]. Less silicon was released from B and P aggregates with KOH and NaOH leading to similar amounts of dissolution (0.2% after 63 days). The higher reactivity of U aggregate can be explained by the petrographic observation of amorphous silica at grain boundaries and the small-sized quartz grains in U aggregate (section 3.2) [31].

The calcium concentrations (see Table A3) were always below the detection limit of ICP–OES. However, calcite dissolution is visible using the scratch-tracking method (section 3.3.1). As high alkali concentration can damage the ICP–OES machine, solutions with high-dilution factor were used for ICP–OES measuring. This limits the measurement precision for minor elements such as Al and Ca, and could explain why the Ca

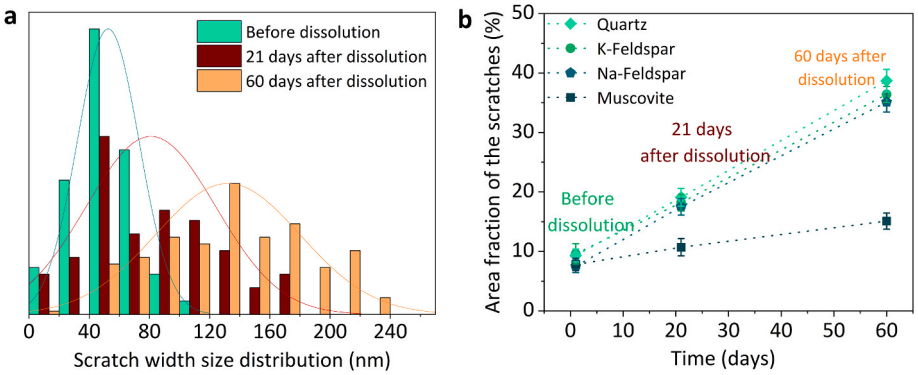

Fig. 6. Quantification of scratch parameters obtained from the alignment of the SEM images of P aggregate; (a) scratch width size distribution (nm) for quartz area and (b) scratch area fraction (%) for quartz, K–feldspar, Na–feldspar and muscovite areas of P aggregate before dissolution, after 21 and 60 days of immersion in 0.4 M KOH solution at 38 °C.

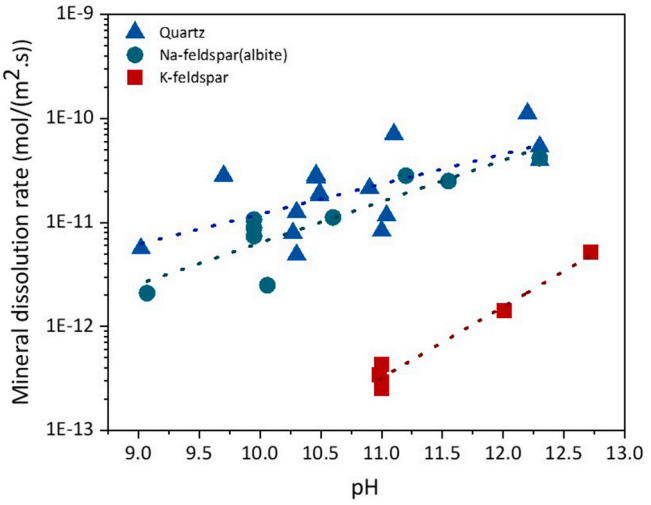

Fig. 7. Dissolution rates of quartz, K–feldspar and Na–feldspar (albite) (mol/(m^2.s)) at high pH (9 < pH < 13) and at 25 °C [7,21–26].

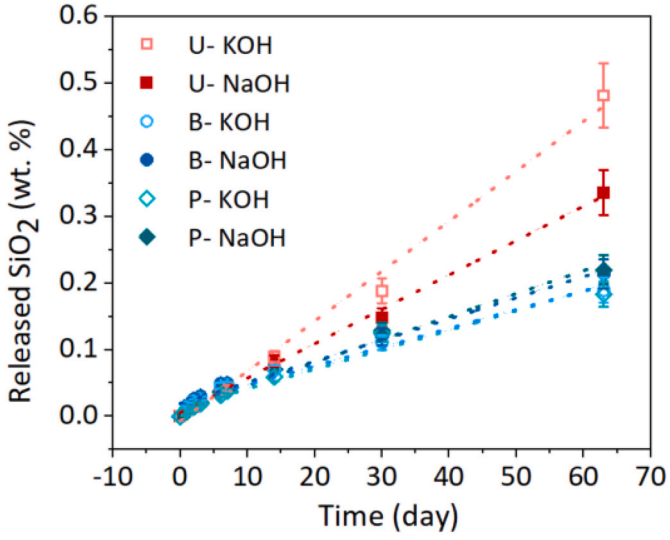

Fig. 8. Released SiO_2 (wt. %) from U, B and P aggregates in 0.4 M KOH and 0.4 M NaOH solutions as a function of time at 38 °C.

concentrations were below the ICP–OES detection limit. The other reason can be formation of new solids (difficult to be detected using XRD due to amorphous structure or TGA (Fig. A5) due to small amount), which consumed the dissolved Ca as indicated by the formation of some products on the surface of samples in the scratch-tracking method, Fig. 4 (c, f and i). It should be noted that, for aggregates with calcite, the measured Si released may be lowered by reaction with Ca from calcite dissolution.

In addition to silicon, Al and alkalis were released in both 0.4 M KOH and 0.4 M NaOH as summarised in Table A3. The concentration of Al increased initially, but then stabilised after 30 days, indicating either a decrease in feldspar dissolution with time and/or precipitation of Al containing solids (Table A3). The highest amount of dissolved Al was observed for the B aggregate, which also contains the highest amount of Al and feldspar as indicated by XRF and XRD/Rietveld analysis (Table 1). A slight increase with time was observed for the measured K or Na concentrations as both the NaOH and KOH solutions used already contained traces of K or Na. However, the small increase of K in the case of NaOH solutions, confirmed the dissolution of K-feldspar in agreement with the results from the scratch-tracking method (section 3.3.1), in particular for the B aggregate with the highest feldspar content. The pH values did not change significantly during the experiments (Table A3).

3.4. Comparison of aggregate dissolution and concrete expansion

The rates of expansion for concrete samples with different aggregates (U, B and P) (%/day) were obtained from the slope of the curves shown in Fig. 2. As the expansion rate of concrete made with U aggregate slightly changed over time (Fig. 2), the initial and constant expansion rate was considered (because the rates of SiO_2 release was measured in short time and up to 2 months). The rates measured in 0.4 M KOH were used, as potassium is the major source of alkali (almost 75%) in the pore solution. Fig. 9 shows the rates of expansion versus the rates of SiO_2 release.

The concrete sample with U aggregate had the highest rate of expansion (%/day) and the highest rate of release of SiO_2 (%/day) in 0.4 M KOH. The concrete samples with B and P aggregates showed almost the same rates of expansion (%/day) and rates of SiO_2 release (%/day) (Fig. 9). As there are essentially only 2 data points in Fig. 9, it would be necessary to study many more aggregates to confirm such a possible general correlation. However, aggregate dissolution in concrete occurs (mainly at the grain boundaries and areas of amorphous or poorly crystalline material) in contact with a limited amount of pore solution, while dissolution experiments are done by immersion of the aggregates in an abundant amount of solution. It was already found that surface area and the distribution of geometric particle diameter play important roles in determining the whole dissolution rates [32,33]. The size

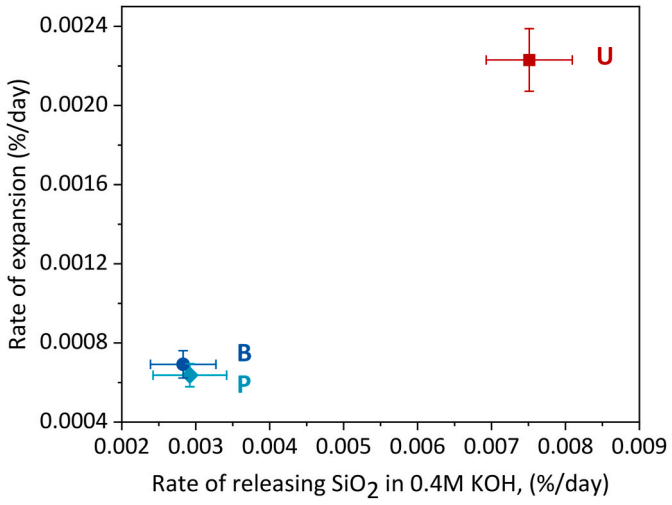

Fig. 9. Rates of expansion of the concrete samples with U, B and P aggregates (%/day) versus rates of releasing SiO_2 from U, B and P aggregates (%/day) in 0.4 M KOH at 38 °C.

fraction of aggregates in concrete is wide, which introduces different surface areas of silica-containing and dissolvable minerals contributing to ASR, while for dissolution experiments a narrow size fraction of aggregates was used. The composition of pore solution in concrete is complex depending on the used paste and aggregates, while simplified solution (0.4 M KOH) was used for dissolution experiments. Some of the critical reactions, such as complex interaction of ASR-gel formation, play a key role in the extent of expansion, and are not considered in dissolution experiments. All of these factors mean that the study of dissolution kinetics only gives an indication of ASR–reactivity of aggregates, and is unlikely to directly related to the extent of expansion across a range of aggregates.

4. Conclusions

In the present study, expansion tests confirmed the ASR susceptibility of three aggregates from Switzerland (U, B and P aggregates). The concrete with U aggregate showed the highest rate of ASR expansion. An innovative scratch-tracking method was introduced to determine reactive minerals within a composite aggregate. This method is a useful approach to monitor reactivity of minerals within aggregate if several minerals, releasing Si/Al, present and formation of new phases causes difficulties to interpret the results of solution analysis based on the amount of released Si. The results based on this method identified quartz, K-feldspar and Na-feldspar as dissolvable minerals within the Swiss aggregates, while the reaction of muscovite was negligible. Investigation of solution composition were done in parallel to study dissolution rates of the aggregates, and to determine the type and the amount of released components (e.g. Si, Al, K and Na) during dissolution reaction. The U aggregate showed the highest rate of release of SiO_2 in the dissolution experiments. It was observed that the type of alkali (NaOH or KOH) only slightly affected the dissolution of the aggregates at 38 °C. This is in agreement with results of dissolution tests using microsilica as a proxy for highly reactive aggregates in NaOH and KOH solutions [4,34]. The release of K/Na, Al and Si confirmed dissolution of feldspars, and therefore, the results based on the scratch-tracking method. These results underline the importance of aggregate dissolution as the first step in expansion due to ASR. Both dissolution experiments and expansion tests revealed higher reactivity of U aggregate in comparison with B and P aggregates. However, a direct correlation between dissolution experiments and expansion tests is not possible given the limited data available from this study. A simple direct correlation across a broad range of aggregates is unlikely due to the complex combination of dissolution, ASR product formation and crack formation involved in damage due to ASR.

Declaration of competing interest

The authors declare that they have no known competing financial interests or personal relationships that could have appeared to influence the work reported in this paper.

Acknowledgements

The authors acknowledge the SNF Sinergia project: Alkali-silica reaction in concrete (ASR), grant number CRSII5_17108 for support of M. Bagheri and M. Shakoorioskooie. We would like to thank Lionel Sofia, Luigi Brunetti and Boris Ingold for their help in some of the experimental work. Swiss Federal Institute of Technology Lausanne (EPFL) and Swiss Federal Laboratories for Materials Science and Technology (Empa) are acknowledged by authors to provide the facilities for the present research.

Appendix

Materials

A Portland cement (CEM I 42.5 N, see Table A1) content of 410 kg/m^3 and a water-to-cement-ratio (w/c) of 0.45 was used for concrete production. The Na_2O-equivalent of the cement was 0.79 kg/m^3 resulting in a total alkali content in the reference concrete (C-Ref) of 3.25 kg/m^3. The aggregate of alluvial origin consisted of gneiss and quartzite. 1790 kg/m^3 of aggregates were added in four different grain size fractions (0/4 mm: 40 mass-%, 4/8 mm: 15 mass-%, 8/16 mm: 20 mass-%, 16/22 mm: 25 mass-%).

Table A1
Composition of CEM I 42.5 N.

Oxides [mass-%]	SiO_2	Al_2O_3	Fe_2O_3	Cr_2O_3	MnO	TiO_2	P_2O_5	CaO	MgO	K_2O	Na_2O	SO_3	LOI
CEM I 42.5	20.14	4.56	3.25	0.013	0.05	0.368	0.24	63.0	1.9	0.96	0.16	3.25	2.06

Three prisms (70 × 70 × 280 mm^3) were produced with each concrete mixture. The prisms were demoulded after 24 h following the protocol of the concrete prism test (CPT) [11].

Method

The concrete prism test according to the Swiss standard SIA 262-1 [11] was used. The test requires storage of the prims (70 × 70 × 280 mm^3) at

60 °C and 100% relative humidity (RH) for 20 weeks with measurements every 4 weeks. The limit value of expansion is 0.20‰.

Result

All concrete prisms showed an expansion between 0.2 and 0.6‰ after 20 weeks (Fig. A1), which are close or above the limit value of 0.20‰ defined in Ref. [11].

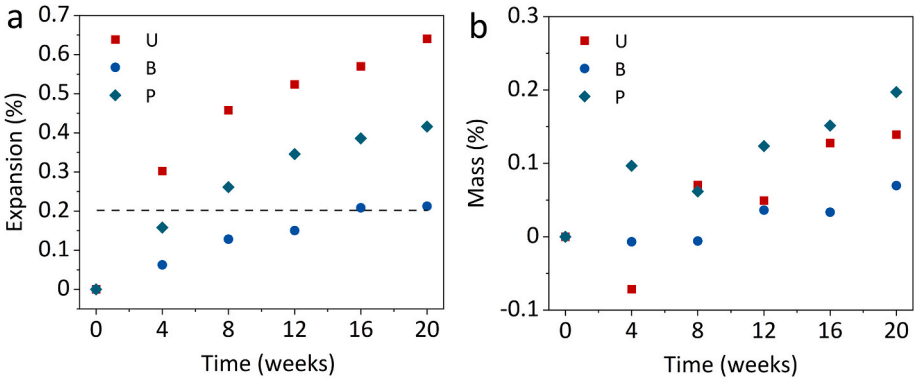

Fig. A1. a) Expansion and b) relative mass change as a function of time of the different concrete mixtures.

Fig. A2. The polished and carbon-coated sample for the scratch-tracking method.

Table A2
(a) XRF and (b) XRD analyses of five crushed subsamples (from a portion of 20 g, 0.315–0.630 mm) of the P aggregate.

Technique	Component	P 1	P 2	P 3	P 4	P5	Standard deviation	Average	Range
XRF (wt. %)	SiO_2	67.6	67.2	66.8	67.6	67.6	0.36	67.4	66.8–67.6
	CaO	12.2	12.4	12.6	12.7	12.1	0.25	12.4	12.1–12.7
	Al_2O_3	4.4	4.4	4.6	4.6	4.5	0.10	4.5	4.4–4.6
	K_2O	1.8	1.8	1.9	1.8	1.8	0.04	1.8	1.8–1.9
	MgO	1.5	1.5	1.5	1.5	1.5	0.00	1.5	1.5
	Fe_2O_3	0.8	0.8	0.8	0.8	0.8	0.00	0.8	0.8
	Na_2O	0.6	0.6	0.6	0.7	0.6	0.04	0.6	0.6–0.7
XRD (wt. %)	**Quartz**: SiO_2 [ICSD 174]	53.1	51.8	55	54.2	52.4	1.30	53.3	51.8–55
	Feldspar: Albite: $NaAlSi_3O_8$ [ICSD 87657]	8.6	7.7	7.7	7.2	8.2	0.54	7.9	7.2–8.6
	Feldspar: Microcline: $KAlSi_3O_8$ [ICSD 83531]	7.4	6.3	6.3	5.6	8	0.96	6.7	5.6–8
	Calcite: $CaCO_3$ [ICSD 73446]	18.6	19.5	18.7	19.2	19	0.37	19.0	18.6–19.5
	Dolomite: $CaMg(CO_3)_2$ [ICSD 66333]	4.8	6.8	5.1	5.5	5.1	0.79	5.5	4.8–6.8
	Mica: Muscovite: $KAl_2(AlSi_3O_{10})(OH)_2$ [ICSD 75952]	7.6	8	7.1	8.3	7.3	0.49	7.7	7.1–8.3

Table A3

(a) Amount of dissolved ions from different aggregates in (a) 0.4 M KOH and (b) 0.4 M NaOH at 38 °C, saturation index values by GEMS and pH values by different methods.

Aggregate	Time (day)	Al (mmol/L)	Ca (mmol/L)	K[(2)] (mmol/L)	Na (mmol/L)	Si (mmol/L)	Sulfate (mmol/L)	Saturation index of C-S-H	Saturation index of SiO_2	pH [(3)]	pH [(4)] (GEMS)
U	0	< LOQ [(1)]	< LOQ	276	3.97	< LOQ	< LOQ	−1.4	−7.4	13.5	12.9
	1	< LOQ	< LOQ	266	3.65	0.173	0.090	−1.0	−5.4	13.5	12.9
	2	< LOQ	< LOQ	269	3.61	0.284	0.095	−1.0	−5.2	13.5	12.9
	3	< LOQ	< LOQ	276	3.98	0.442	0.113	−0.9	−5.0	13.5	12.9
	6	< LOQ	< LOQ	289	4.11	0.787	8.833	−0.9	−4.7	13.5	12.9
	7	< LOQ	< LOQ	309	4.39	0.958	0.158	−0.8	−4.7	13.4	12.9
	14	0.196	0.048	327	3.04	2.136	0.287	−0.3	−4.3	13.5	13.0
	30	0.393	< LOQ	338	4.39	4.771	0.636	−0.7	−4.0	13.5	13.0
	63	0.272	< LOQ	394	5.44	12.926	3.779	−0.6	−3.5	13.4	13.0
B	0	< LOQ	< LOQ	276	3.97	< LOQ	< LOQ	−1.4	−7.4	13.5	12.9
	1	0.247	< LOQ	279	3.78	0.237	0.112	−1.0	−5.3	13.5	12.9
	2	0.332	< LOQ	297	4.04	0.392	0.114	−0.9	−5.1	13.5	12.9
	3	0.471	< LOQ	276	3.75	0.477	0.092	−0.9	−5.0	13.4	12.9
	6	0.519	0.129	338	4.65	0.876	1.199	−0.2	−4.7	13.4	13.0
	7	0.526	0.131	320	4.65	0.933	0.145	−0.2	−4.7	13.4	13.0
	14	0.650	0.058	322	3.11	1.453	0.098	−0.4	−4.5	13.5	13.0
	30	0.967	< LOQ	338	4.39	2.439	0.195	−0.7	−4.3	13.5	13.0
	63	1.056	< LOQ	389	5.44	4.415	1.291	−0.7	−4.0	13.5	13.0
P	0	< LOQ	< LOQ	276	3.97	< LOQ	< LOQ	−1.4	−7.4	13.5	12.9
	1	< LOQ	< LOQ	271	3.70	0.148	0.101	−1.1	−5.5	13.5	12.9
	2	< LOQ	< LOQ	286	3.95	0.271	0.111	−1.0	−5.2	13.4	12.9
	3	< LOQ	< LOQ	269	3.80	0.388	0.106	−1.0	−5.1	13.4	12.9
	6	< LOQ	< LOQ	294	4.19	0.677	0.151	−0.9	−4.8	13.4	12.9
	7	< LOQ	< LOQ	332	4.52	0.840	0.148	−0.8	−4.7	13.4	13.0
	14	0.053	0.052	284	2.70	1.390	0.089	−0.4	−4.5	13.4	12.9
	30	0.203	< LOQ	345	4.19	3.080	0.231	−0.7	−4.2	13.5	13.0
	63	< LOQ	< LOQ	353	4.57	4.807	1.405	−0.7	−4.0	13.5	13.0

Aggregate	**Time (day)**	**Al (mmol/L)**	**Ca (mmol/L)**	**K (mmol/L)**	**Na [(2)] (mmol/L)**	**Si (mmol/L)**	**Sulfate (mmol/L)**	**Saturation index of C-S-H**	**Saturation index of SiO_2**	pH [(3)]	pH [(4)] (GEMS)
U	0	< LOQ[(1)]	< LOQ	0.30	326	< LOQ	< LOQ	−1.3	−7.1	13.1	12.9
	1	< LOQ	< LOQ	0.44	340	0.227	0.092	−0.9	−5.1	13.1	13.0
	2	< LOQ	< LOQ	0.53	345	0.377	0.102	−0.8	−4.9	13.1	13.0
	3	< LOQ	< LOQ	0.52	327	0.499	0.101	−0.8	−4.8	13.1	12.9
	6	0.211	< LOQ	0.58	334	0.858	0.124	−0.8	−4.5	13.1	12.9
	7	0.225	< LOQ	0.59	355	0.983	0.162	−0.7	−4.5	13.1	13.0
	14	0.284	0.047	0.72	352	1.994	0.187	−0.3	−4.2	13.1	13.0
	30	0.486	< LOQ	0.65	362	3.739	0.445	−0.6	−4.0	13.1	13.0
	63	0.448	< LOQ	0.95	428	9.009	2.634	−0.1	−3.7	13.1	13.0
B	0	< LOQ	< LOQ	0.30	326	< LOQ	< LOQ	−1.3	−7.1	13.1	12.9
	1	0.263	< LOQ	0.34	336	0.275	0.100	−0.9	−5.0	13.1	13.0
	2	0.361	< LOQ	0.47	340	0.445	0.103	−0.8	−4.8	13.1	13.0
	3	0.404	< LOQ	0.54	327	0.548	0.107	−0.8	−4.7	13.1	12.9
	6	0.615	< LOQ	0.70	386	0.922	0.130	−0.7	−4.6	13.1	13.0
	7	0.641	< LOQ	0.78	389	0.976	0.126	−0.7	−4.6	13.1	13.0
	14	0.788	0.053	0.92	376	1.462	0.078	−0.3	−4.4	13.1	13.0
	30	1.245	< LOQ	0.92	414	2.628	0.198	−0.5	−4.2	13.1	13.0
	63	1.490	< LOQ	1.21	444	4.985	1.457	−0.4	−4.0	13.1	13.0
P	0	< LOQ	< LOQ	0.30	326	< LOQ	< LOQ	−1.3	−7.1	13.1	12.9
	1	0.201	< LOQ	2.05	323	0.132	0.086	−0.9	−5.3	13.1	12.9
	2	< LOQ	< LOQ	0.42	329	0.280	0.105	−0.9	−5.0	13.1	12.9
	3	< LOQ	< LOQ	0.54	335	0.438	0.117	−0.8	−4.8	13.1	13.0
	6	< LOQ	< LOQ	0.64	358	0.787	0.133	−0.8	−4.6	13.1	13.0
	7	< LOQ	< LOQ	0.89	398	0.947	0.126	−0.7	−4.6	13.1	13.0
	14	0.090	0.059	0.91	385	1.661	0.095	−0.3	−4.4	13.1	13.0
	30	0.264	< LOQ	0.91	406	3.183	0.232	−0.6	−4.1	13.2	13.0
	63	0.154	< LOQ	1.20	386	5.768	1.686	−0.6	−3.8	13.1	12.8

(1) LOQ = Limit of Quantification. LOQ (Al, Na and Si) = 0.02 mmol/L; and LOQ (Ca, K and Sulfate) = 0.01 mmol/L.

(2) The ICP-OES results are underestimated due to presence of strong alkali content.

(3) The pH values were measured at room temperature ~ 23 °C.

(4) The pH values by GEMS are at 38 °C, and pH of 0.4 M KOH equals to 13.5 at 23 °C and to 13.0 at 38 °C.

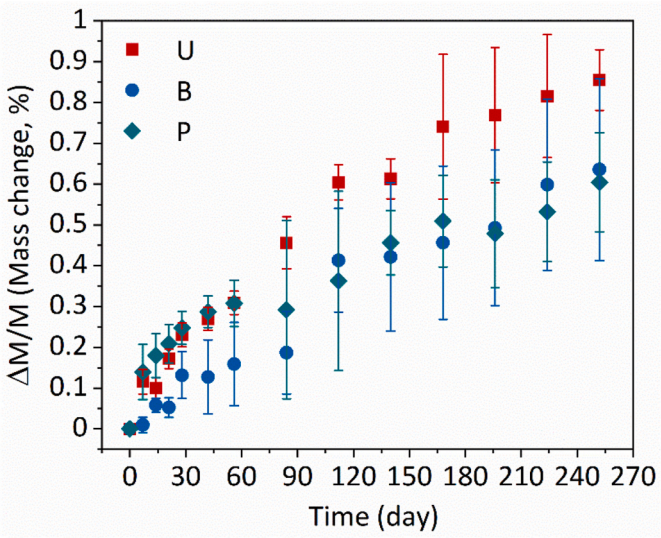

Fig. A3. Mass change (%) of concrete samples with U, b and P aggregates as a function of time.

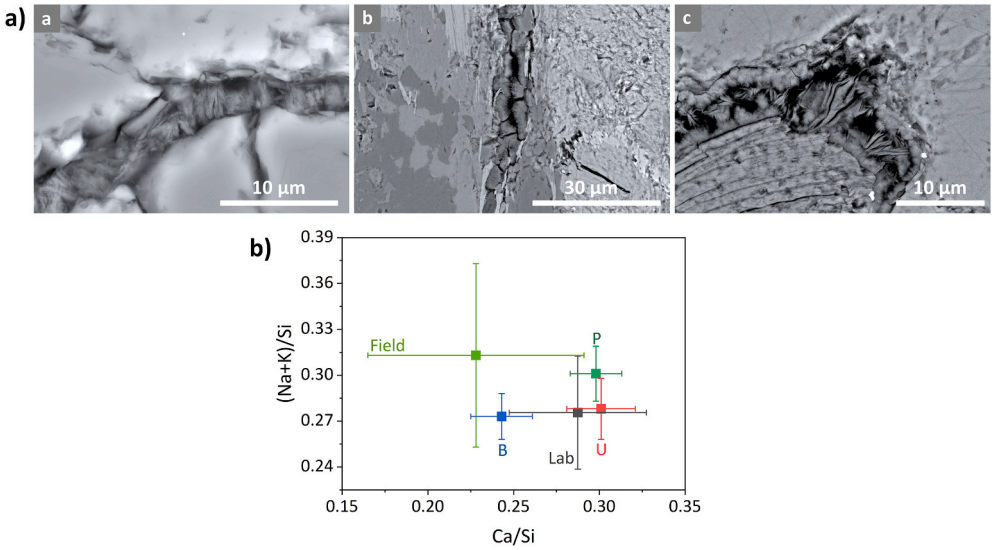

Fig. A4. (a) SEM backscattered images and (b) EDX analysis of ASR products in concrete samples with (a) P, (b) B and (c) U aggregates after 250 days compared to compositions reported for field and laboratory samples from [19].

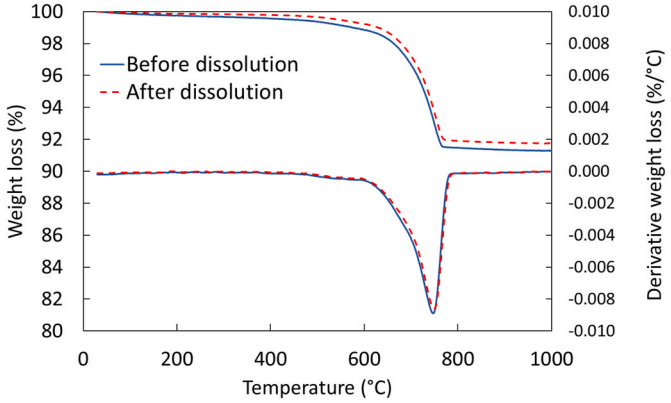

Fig. A5. Thermogravimetric analysis of U aggregate (solid line) and of the collected solids at the end of dissolution experiments (dash line) in 0.4 M NaOH at 38 °C.

References

[1] T. Chappex, K. Scrivener, Alkali fixation of C-S-H in blended cement pastes and its relation to alkali silica reaction, Cem. Concr. Res. 42 (2012) 1049–1054, https://doi.org/10.1016/j.cemconres.2012.03.010.

[2] L.S. Dent Glasser, N. Kataoka, The chemistry of "alkali-aggregate" reaction, Cem. Concr. Res. 11 (1981) 1–9.

[3] F. Rajabipour, E. Giannini, C. Dunant, J.H. Ideker, M.D.A. Thomas, Alkali-silica reaction: current understanding of the reaction mechanisms and the knowledge gaps, Cem. Concr. Res. 76 (2015) 130–146, https://doi.org/10.1016/j.cemconres.2015.05.024.

[4] A. Leemann, L. Lörtscher, L. Bernard, G. Le Saout, B. Lothenbach, R.M. Espinosa-Marzal, Mitigation of ASR by the use of LiNO3 - characterization of the reaction products, Cem. Concr. Res. 59 (2014) 73–86, https://doi.org/10.1016/j.cemconres.2014.02.003.

[5] T. Chappex, K.L. Scrivener, The effect of aluminum in solution on the dissolution of amorphous silica and its relation to cementitious systems, J. Am. Ceram. Soc. 96 (2013) 592–597, https://doi.org/10.1111/jace.12098.

[6] S. Chatterji, Chemistry of alkali – silica reaction and testing of aggregates, Cem. Concr. Compos. 27 (2005) 788–795, https://doi.org/10.1016/j.cemconcomp.2005.03.005.

[7] S.L. Brantley, A.F. White, J.D. Kubicki, Kinetics of Water-Rock Interaction, Springer, New York (2008), https://doi.org/10.1007/978-0-387-73563-4.

[8] A. Leemann, L. Holzer, Alkali-aggregate reaction-identifying reactive silicates in complex aggregates by ESEM observation of dissolution features, Cem. Concr. Compos. 27 (2005) 796–801, https://doi.org/10.1016/j.cemconcomp.2005.03.007.

[9] G. Yuan, Y. Cao, H. Schulz, F. Hao, J. Gluyas, K. Liu, A review of feldspar alteration and its geological significance in sedimentary basins: from shallow aquifers to deep hydrocarbon reservoirs, Earth Sci. Rev. (2019), https://doi.org/10.1016/j.earscirev.2019.02.004.

[10] W. Stumm, J.J. Morgan, Aquatic Chemistry: Chemical Equilibria and Rates in Natural Waters, American Library Association, 1996, https://doi.org/10.5860/choice.33-6312.

[11] SIA 2042 262-1. Betonbau – Ergänzende Festlegungen. Anhang G: Alkali-Aggregat-Reaktionswiderstand (AAR): Performance-Methode, SIA, Zurich, 2019.

[12] A. Leemann, B. Münch, The addition of caesium to concrete with alkali-silica reaction: implications on product identification and recognition of the reaction sequence, Cement Concr. Res 120 (2019) 27–35, https://doi.org/10.1016/j.cemconres.2019.03.016.

[13] A. Leemann, Impact of different added alkalis on concrete expansion due to ASR, Proc. 16th Int. Conf. Alkali-Aggregate React. Concr. (2021) 175–184.

[14] M.J. Tapas, L. Sofia, K. Vessalas, P. Thomas, V. Sirivivatnanon, K. Scrivener, Efficacy of SCMs to mitigate ASR in systems with higher alkali contents assessed by pore solution method, Cem. Concr. Res. 142 (2021), 106353, https://doi.org/10.1016/j.cemconres.2021.106353.

[15] B.C. Lowekamp, D.T. Chen, L. Ibáñez, D. Blezek, The design of SimpleITK, Front. Neuroinform. 7 (2013) 1–14, https://doi.org/10.3389/fninf.2013.00045.

[16] C. Bärtschi, Kieselkalke der Schweiz: Charakterisierunq eines Rohstoffs aus geologischer, petroqraphischer, wirtschaftlicher und umweltrelevanter Sicht, Beitr. Geol. Schweiz. Geotechn. 97 (2012) 1–160.

[17] ASTM C1293, Standard test method for determination of length change of concrete due to alkali-silica reaction, Annu. Book ASTM Stand. 04.02 (n.d.). doi:10.1520/C1293-20A.2.

[18] Canadian Standard CSA, A23.2-14A Potential expansivity of aggregates (procedure for length change due to alkali-aggregate reaction in concrete, prisms at 38 °C). Methods of Testing for Concrete, Mississauga, Canadian Standards Association, Ontario, Canada, pp. 246–256.

[19] A. Leemann, I. Borchers, M. Shakoorioskooie, M. Griffa, C. Müller, P. Lura, Microstructural analysis of ASR in concrete-accelerated testing versus natural exposure, In Proc. Pro128 Int. Conf. Sustain. Mater. Syst. Struct.(SMSS2019). Durability, Monit. Repair Struct. RILEM Publ. SARL, Paris, Fr. Rilem Publications, Paris. (2019) 222–229.

[20] A. Leemann, Z. Shi, J. Lindgård, Characterization of amorphous and crystalline ASR products formed in concrete aggregates, Cem. Concr. Res. 137 (2020) 106190, https://doi.org/10.1016/j.cemconres.2020.106190.

[21] P.M. Dove, S.F. Elston, Dissolution kinetics of quartz in sodium chloride solutions: analysis of existing data and a rate model for 25°C, Geochem. Cosmochim. Acta 56 (1992) 4147–4156, https://doi.org/10.1016/0016-7037(92)90257-J.

[22] R. Wollast, L. Chou, in: A. Lerman, M. Maybeck (Eds.), In Physical and Chemical Weathering in Geochemical Cycles, Springer Netherlands, 1988, https://doi.org/10.1007/978-94-009-3071-1.

[23] P.V. Brady, J.V. Walther, Kinetics of quartz dissolution at low temperatures, Chem. Geol. 82 (1990) 253–264, https://doi.org/10.1016/0009-2541(90)90084-K.

[24] W.A. House, D.R. Orr, Investigation of the pH dependence of the kinetics of quartz dissolution at 25°C, J. Chem. Soc., Faraday Trans. 88 (1992) 233–241, https://doi.org/10.1039/FT9928800233.

[25] L. Chou, R. Wollast, Steady-state kinetics and dissolution mechanisms of albite, Am. J. Sci. 285 (1985) 963–993, https://doi.org/10.2475/ajs.285.10.963.

[26] K.G. Knauss, T.J. Wolery, Dependence of albite dissolution kinetics on pH and time at 25°c and 70°c, Geochem. Cosmochim. Acta 50 (1986) 2481–2497, https://doi.org/10.1016/0016-7037(86)90031-1.

[27] K. Lammers, M.M. Smith, S.A. Carroll, Muscovite dissolution kinetics as a function of pH at elevated temperature, Chem. Geol. 466 (2017) 149–158, https://doi.org/10.1016/j.chemgeo.2017.06.003.

[28] E.H. Oelkers, J. Schott, J. Gauthier, T. Herrero-roncal, An experimental study of the dissolution mechanism and rates of muscovite, Geochim. Cosmochim. Acta 72 (2008) 4948–4961, https://doi.org/10.1016/j.gca.2008.01.040.

[29] P.M. Dove, C.J. Nix, The influence of the alkaline earth cations, magnesium, calcium, and barium on the dissolution kinetics of quartz, Geochem. Cosmochim. Acta 61 (1997) 3329–3340, https://doi.org/10.1016/S0016-7037(97)00217-2.

[30] S. Plettinck, L. Chou, R. Wollast, Kinetics and mechanisms of dissolution of silica at room temperature and pressure, Mineral. Mag. 58A (1994) 728–729, https://doi.org/10.1180/minmag.1994.58a.2.116.

[31] D. De Paiva Gomes Neto, H. Conceição, V.A.C. Lisboa, R.S. De Paiva Santana, L. S. Barreto, Influence of granitic aggregates from Northeast Brazil on the alkali-aggregate reaction, Mater. Res. 17 (2014) 51–58, https://doi.org/10.1590/S1516-14392014005000045.

[32] Y. Niibori, M. Kunita, O. Tochiyama, T. Chida, Dissolution rates of amorphous silica in highly alkaline solution, J. Nucl. Sci. Technol. 37 (2000) 349–357, https://doi.org/10.1080/18811248.2000.9714905.

[33] J.M. Gautier, E.H. Oelkers, J. Schott, Are quartz dissolution rates proportional to B. E.T. surface areas? Geochem. Cosmochim. Acta 65 (2001) 1059–1070, https://doi.org/10.1016/S0016-7037(00)00570-6.

[34] A. Leemann, G. Le Saout, F. Winnefeld, D. Rentsch, B. Lothenbach, Alkali–silica reaction: the influence of calcium on silica dissolution and the formation of reaction products, J. Am. Ceram. Soc. 94 (2011) 1243–1249, https://doi.org/10.1111/J.1551-2916.2010.04202.X.